Soft, Flexible Freestanding Neural Stimulation and Recording Electrodes Fabricated from Reduced Graphene Oxide

*Nicholas V. Apollo, Matias I. Maturana, Wei Tong, David A. X. Nayagam, Mohit N. Shivdasani, Javad Foroughi, Gordon G. Wallace, Steven Prawer, Michael R. Ibbotson, and David J. Garrett**

There is an urgent need for conductive neural interfacing materials that exhibit mechanically compliant properties, while also retaining high strength and durability under physiological conditions. Currently, implantable electrode systems designed to stimulate and record neural activity are composed of rigid materials such as crystalline silicon and noble metals. While these materials are strong and chemically stable, their intrinsic stiffness and density induce glial scarring and eventual loss of electrode function in vivo. Conductive composites, such as polymers and hydrogels, have excellent electrochemical and mechanical properties, but are electrodeposited onto rigid and dense metallic substrates. In the work described here, strong and conductive microfibers (40–50 µm diameter) wet-spun from liquid crystalline dispersions of graphene oxide are fabricated into freestanding neural stimulation electrodes. The fibers are insulated with parylene-C and laser-treated, forming "brush" electrodes with diameters over 3.5 times that of the fiber shank. The fabrication method is fast, repeatable, and scalable for high-density 3D array structures and does not require additional welding or attachment of larger electrodes to wires. The electrodes are characterized electrochemically and used to stimulate live retina in vitro. Additionally, the electrodes are coated in a water-soluble sugar microneedle for implantation into, and subsequent recording from, visual cortex.

1. Introduction

Devices that are capable of high fidelity and long-term communication with the nervous system have the potential to address some of the most debilitating medical conditions. There are several successful examples of such bionic, or cyberonic, devices including the cochlear implant,[1] cochlear nucleus prosthesis,[2] retinal prosthesis,[3] brain–machine interface (BMI),[4] and deep brain stimulation (DBS) electrodes for the treatment of conditions, including depression, essential tremor, chronic pain, and epilepsy.[5] For some of these devices, there is potential benefit in increasing the spatial resolution of stimulation and/or recording, in particular for retinal prostheses and BMIs. High-resolution electrical communication with the nervous system is a nontrivial task, especially in applications that involve long-term passive recording of neural activity.[6] Insertion of electrodes into the brain leads to damage of blood vessels, capillaries, and cells, and breaches the highly selective blood–brain barrier (BBB).[7] Less destructive noninvasive neural recording techniques such as fMRI, fNIRS, and EEG avoid tissue reactions at the expense of spatial and temporal resolution and are not currently portable; therefore, they are not suitable for BMI applications.[8] Additionally, none of these methods is capable of stimulating neural tissue.

Penetrating electrodes inevitably cause some degree of damage during insertion. Options to avoid invasive surgery will likely come from optogenetic solutions in which light-sensitive molecules are incorporated into the membranes of excitable cells.[9] It has been suggested that the initial electrode implantation site may heal over time, but it is the long-term presence of a foreign object that leads to poor prognosis for chronic recording applications. In other words, the initial "stab wound" will heal eventually, but it is the long-term irritation, and subsequent cellular activation, at the implant site that leads to loss of the electrode–neuron interface.[10] However, two-photon imaging has been used to show an immediate microglial response to electrode insertion, whereby microglial cells extended processes toward the electrode within 30–45 min and began the transition to their "frustrated" phenotype (T-cell

N. V. Apollo, W. Tong, Prof. S. Prawer, Dr. D. J. Garrett
Department of Physics
University of Melbourne
Parkville, VIC 3010, Australia
E-mail: dgarrett@unimelb.edu.au
N. V. Apollo, Dr. D. A. X. Nayagam,
Dr. M. N. Shivdasani, Dr. D. J. Garrett
The Bionics Institute
384-388 Albert Street, East Melbourne, VIC 3002, Australia
M. I. Maturana, Prof. M. R. Ibbotson
National Vision Research Institute
Australian College of Optometry
Carlton, VIC 3053, Australia
Dr. D. A. X. Nayagam
Department of Pathology
The University of Melbourne
Parkville, VIC 3010, Australia
Dr. J. Foroughi, Prof. G. G. Wallace
Intelligent Polymer Research Institute, ARC Centre of Excellence for Electromaterials Science
AIIM Facility, Innovation Campus
University of Wollongong
North Wollongong, NSW 2522, Australia

DOI: 10.1002/adfm.201500110

mode) after 6 h.[11] Initial damage sends the signal for microglial activation and migration to the implantation site, which, if tissue irritation continues, progresses until microglia form the dense glial sheath that is a familiar detriment to chronic neural communication.[7] Additionally, long-term breach of the highly selective BBB eventually leads to secretion of neurotoxins that kill neurons proximal to the electrode, thereby diminishing the signal of interest permanently.[12]

Contributing factors believed to adversely affect the quality of the electrode–tissue interface in a chronic time window include electrode size,[13,14] density of electrode material,[15] skull tethering mechanisms and associated micromotion of the implant,[16] and mechanical compliance of the electrode itself.[17,18] Considering the aforementioned characteristics, the ideal implantable electrode will be small, soft, mechanically strong, and have a density similar to neural tissue. Present implantable electrodes are made from rigid materials such as noble metals, stainless steel, or crystalline silicon, though the density and stiffness of these materials render them nonideal for chronic interaction with neural tissue.

A soft, flexible electrode has the potential to stifle the foreign body response, but presents a new challenge: surgical insertion. Flexible fibers have been inserted into tissue using dissolvable coatings such as gelatin,[19] silk,[20] and maltose.[21] Carbon nanotube bundle electrodes on flexible substrates have been inserted into the brain using a rigid gold wire carrier.[22] In addition to favorable mechanical properties, the surface chemistry of implanted electrodes has been studied to enhance biocompatibility. Functionalization with, or simultaneous administration of, penetrating electrodes with anti-inflammatory agents,[23] anti-oxidants,[24] neurogenic factors,[25] zwitterionic hydrogels,[26] and bioactive conducting polymers[27] has also been proposed to attenuate the foreign body response to implanted devices. In terms of device hardware, untethered and fully wireless cortical implants have been developed to alleviate displacement-induced strain and shear forces at the electrode–tissue interface.[28]

The availability of low-density and high-strength makes carbon-based materials such as graphene and carbon nanotubes promising candidates as implantable electrode materials. Several carbonaceous materials have seen wide application as successful biomaterials.[29] Some examples of application include graphene for cell scaffolds,[30] carbon fiber dopamine sensors,[31] carbon fiber neural recording devices,[25,32] carbon nanotube neural recording devices,[33] carbon nanotube/agarose hybrid materials for tissue engineering,[34] and nitrogen-doped diamond stimulating electrodes.[35] Two recent publications describe graphene oxide (GO) conductive polymer hybrid films as successful neural interfacing electrodes.[36,37] The more recent of the two, by Tian et al., describes electrochemical deposition of a poly(3,4-ethylenedioxythiophene)/graphene oxide (PEDOT/GO) hybrid film onto gold wires (100 µm diameter).[37] The coating demonstrated enhanced and robust electrochemical properties in comparison to iridium oxide and supported cell growth. It has been shown previously that nonsmooth electrodes, such as conductive polymers and porous or roughened surfaces, are likely to enhance the quality of the neural interface by reducing the fluid gap between electrode and tissue and by reducing the electrical impedance and increasing the capacitance at the electrode tissue interface.[27]

A risk with hybrid metal/polymer structures is that they are prone to failure in chronic settings due to material density and mechanical compliance mismatch with brain tissue. For long-term applications, it is perhaps more suitable to have the entire electrode and connection wire made of one flexible and strong material—a freestanding electrode/wire system. Additionally, as electrodes get smaller (≤200 µm diameter)—to improve stimulation efficacy of retinal ganglion cells (RGCs), for example—wire-to-electrode attachment becomes a significant challenge.[38] For the work described in this article, we chose reduced graphene oxide fibers because they are facile to produce into long continuous yarns and avoid the common issues of electrical attachment that other carbonaceous materials face.

In this work, we propose a new neural interfacing electrode material and configuration that is assessed using techniques specific to neuronal stimulation. We describe a unique "brush" electrode composed of wet-spun liquid crystal graphene oxide (LCGO) fiber and parylene-C insulation. A 532 nm laser cutter is used to open the insulation and remove the end of the fiber, forming a brush-like electrode at the end of the shank that is roughly 3.5 times larger than the shank itself and appears to have an exceptionally large real surface area. Laser excimer procedures have been used previously to reduce thin films of GO to enhance electrical conductivity.[39] However, in this work, the entire fiber is thermally reduced before electrode fabrication begins to ensure optimal electrical conductivity through the shank.[40] Following electrochemical characterization, the electrodes are used to stimulate rat RGCs during whole cell patch clamp recordings and coated in a water-soluble sucrose microneedle to penetrate visual cortex to enable acquisition of high quality neural signals.

2. Results and Discussion

2.1. Electrode Fabrication

Long (>10 m), conductive (30 mS cm^{-2}) fibers were wet-spun from liquid crystalline (LC) dispersions of GO (Figure S1, see Supporting Information) and reduced in vacuum at 220 °C.[40] The LC state of the dispersion greatly enhances the spinnability of the fibers, as well as the mechanical properties.[40] LCGO fibers coagulated with $CaCl_2$ have a Young's modulus of 11.2 GPa, whereas crystalline silicon and Pt have Young's moduli as high as 168 GPa and 47 GPa, respectively. It has been suggested previously that both size and elastic modulus play a role in the extent of glial scarring around brain implants, whereby 50 µm diameter implants lead to less extensive foreign body reaction and greater proximal neuron survival compared with a 200 µm implant.[14] Larger electrode leads, such as those currently used for commercially available implantable electrode systems, will have much greater stiffness values due to both the increased size and higher elastic modulus of the materials used to build those devices.

Stimulation electrodes for electrochemical characterization and electrophysiology experiments were fabricated using 8–10 mm of reduced LCGO fiber (**Figure 1**). The entire electrode was coated with parylene-C (a polymer well known for its biocompatibility and pin-hole free coatings for electronics packages and neural prostheses[41] and then laser ablated to create an open electrode at the end (Figure 1c). The laser ablation approach did not work for a parylene-C-coated PtIr wire due to the high powers required to sever the wire (Figure S2, see Supporting Information). Laser ablation has been used previously to selectively remove parylene-C from the electrode tips of the UTAH (Blackrock Microsystems) neural recording array.[42] In that instance, the electrodes themselves remained intact following laser treatment.

Using LCGO fibers as the electrode material, low laser powers (230–250 mW) cut through both the coating and the fiber. At the low laser powers used in this work, the laser must be accurately focused on an individual fiber to ablate it, leaving out-of-focus fibers untouched. For 3D arrays, shaping and insulation removal may be controlled by simply adjusting the laser focus to ablate individual fibers. The mechanical properties of the brush electrode are retained following the fabrication steps as illustrated in **Figure 2**.

Figure 2a shows an electrode pushed into a piece of clay until it was nearly bent in half, and then retracted (Figure 2b), restoring its original shape and, hence, demonstrating elastic deformation. Elasticity was enhanced with parylene-C coating. The expanded and, therefore less dense, end of the brush electrode is potentially much softer than the original fiber. If the electrode itself is much softer, there is a greater chance of neuronal integration and diminished chance of glial activation at the interface.[18] As a result, the electrode is too soft for direct insertion into neural tissue. Hence, we have coated the electrode in a water-soluble sucrose microneedle to provide the mechanical stability for surgical implantation (Figure 2d). This technique has been demonstrated elsewhere for transdermal drug delivery, as well as mechanical support for a polyimide neural probe.[21,43] The needle shown in Figure 2d dissolved in approximately 3 min time in room temperature tap water resulting in the exposed LCGO electrode shown in Figure 2e.

The major point of interest in this fabrication technique lies in the ability to form a large surface area electrode at the end of a small wire generating a continuous, flexible, and freestanding neural probe with no need for welding or bonding of a larger electrode.

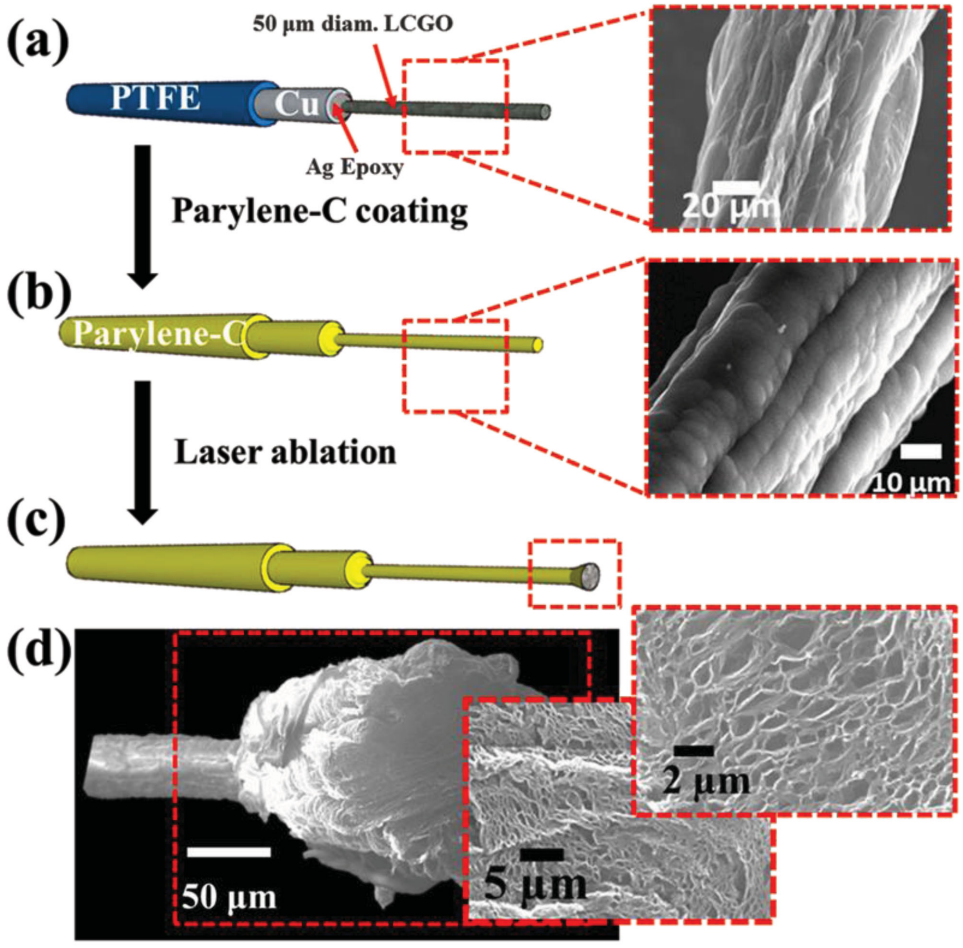

Figure 1. Fabrication and imaging of LCGO brush electrodes. a) LCGOs are attached to PTFE (insulated) insulated copper wires (approximately 1 mm diameter) using conductive silver-based epoxy, followed by b) parylene-C coating. c) Laser ablation with 250 mW opens the electrode end, creating a "brush" electrode. d) Laser treatment leads to an amorphous electrode with extraordinary surface roughness and porosity.

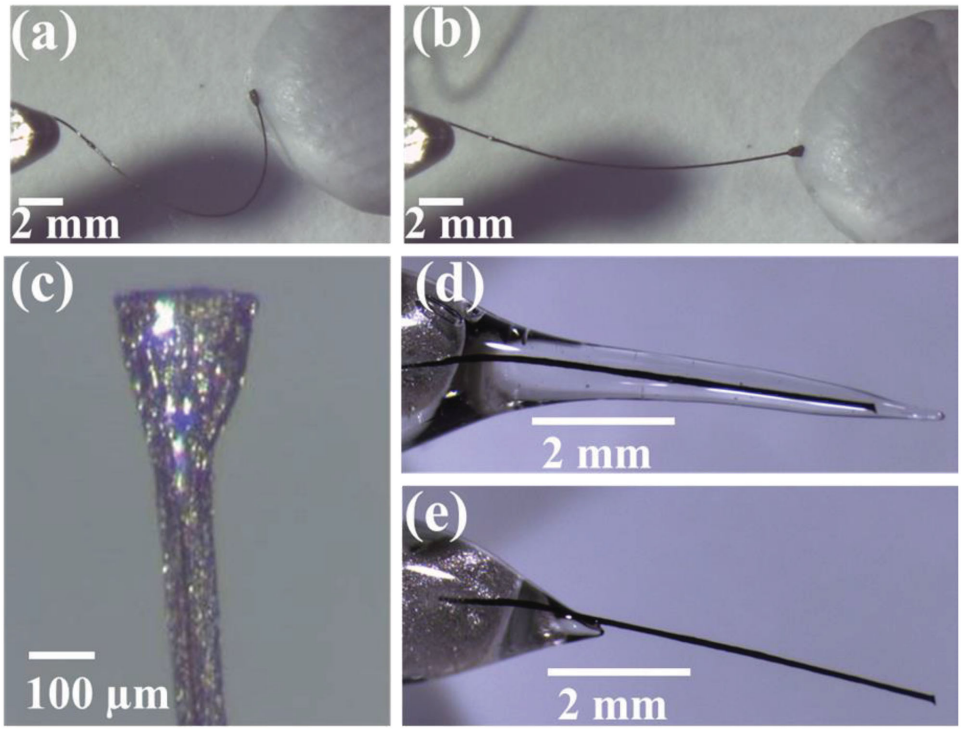

Figure 2. LCGO electrode pressed into clay a) and released b) to demonstrate flexibility and elastic deformation. c) High magnification microscope image of electrode tip following laser ablation. d) LCGO fiber (not laser ablated) encased in sucrose microneedle and e) dissolved microneedle after 3 min in room temperature tap water.

2.2. Electrochemical Characterization

Electrochemical impedance spectroscopy (EIS) and cyclic voltammetry (CV) were acquired using 50×10^{-3} M PBS as the electrolyte and a three-electrode electrochemical cell.

EIS spectra acquired from parylene-C-coated samples could not be fitted to any simple equivalent circuit due to the high impedance of the coating, resulting in current magnitudes that were close to the noise level of the measuring equipment. The phase angle of parylene-C-coated LCGO wires at 100 kHz was –86° ± 4.2°, a nearly entirely capacitive response at high frequency, confirming a pinhole-free, high impedance parylene-C coating. Laser ablation of the fiber led to a 1000-fold drop in electrode/solution impedance and the phase angle at 100 kHz dropped to –13° ± 1.6°. Following EIS sweeps, a linear equivalent circuit was used to fit the data and extract capacitance and series resistance values. The linear circuit (**Figure 3**b, inset) contains a series resistance (R_s) and a constant phase element (CPE). A CPE is used to model electrochemical behavior of electrodes that have surface inhomogeneity, such as fractal or porous electrodes.[44] LCGO fibers have extremely large surface roughness and nano-porosity following laser ablation as evidenced by scanning electron microscopy (SEM) (Figure 1d). Geometric surface area (GSA) values have been used for all capacitance and charge injection capacity calculations. Attempts to confidently estimate real surface area have, to date, been unsuccessful. However, considering the low fundamental capacitance values measured for basal plane the surface area enhancement could be very high.[45] Additionally, it is likely that small pockets have opened up between the parylene-C and LCGO fiber near the electrode—an effect possibly exaggerated by CV scans. Manufacturers of parylene-C quote a dielectric strength of 220 volts µm^{-1}, meaning that for a 2 µm film, 440 V would be required to breach insulation (VSI Parylene, Inc.). For CV scans between –600 and 600 mV, residual parylene-C films of 200–300 nm thickness would be removed assuming laser treatment does not change the chemical structure of the polymer. It has been shown that thermal treatment of parylene-C can increase bonding strength to substrates, which will have an effect at the end of the electrode following laser treatment.[46]

Using EIS and circuit modeling, a double layer capacitance (C_{dl}) value was extracted for LCGO electrodes of 16 ± 1 µF. Charge injection capacity (Q_{inj}) was calculated using the following:

$$Q_{inj} = \frac{C_{dl} \times V_w}{GSA} \quad (1)$$

where V_w is the voltage threshold to electrolysis (+0.9 V for LCGO) and GSA is the GSA of the electrode tip assuming only a disc electrode is exposed to the solution. This yielded an extraordinarily high Q_{inj} of 46 ± 2.9 mC cm^{-2}. It is highly likely that charge transfer is occurring not only at a disc electrode at the tip, but likely within the parylene-C sheath, as well as on the outside of the brush. Hence, the Q_{inj} value is potentially artificially inflated. LCGO electrodes do not have a uniform geometric shape as a result of both the wet-spinning and the laser fabrication technique. To improve this estimation, we model the GSA of the brush electrode using a GSA based on either a disc electrode or a larger cone electrode (Figure S3,

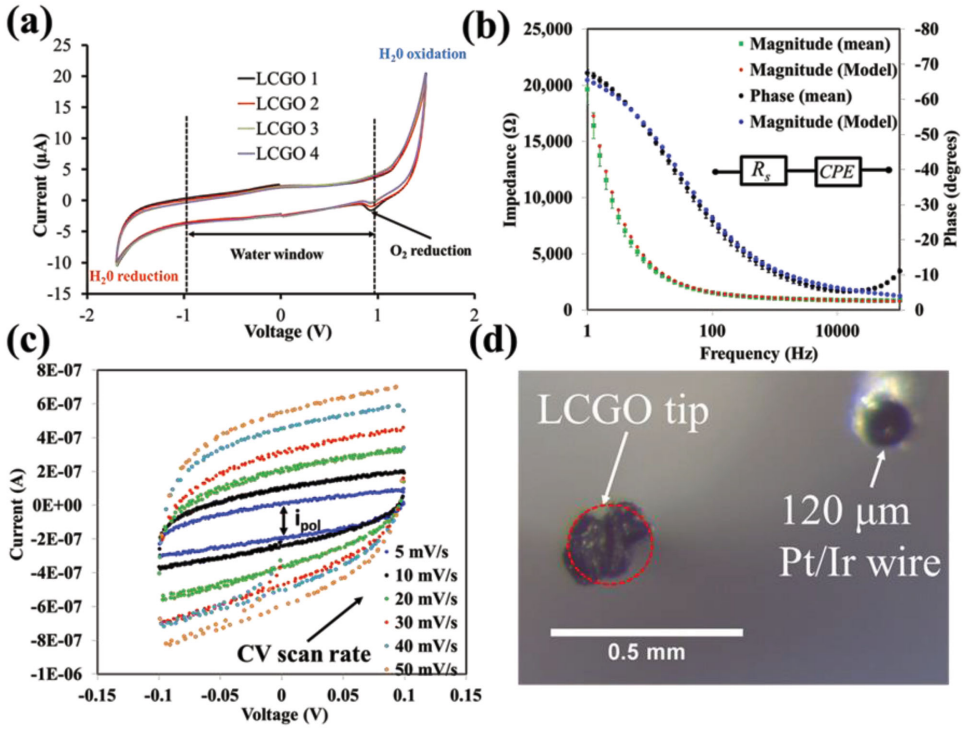

Figure 3. a) Cyclic voltammograms for four LCGO electrodes fabricated using the same laser parameters as those employed for both in vitro and in vivo experiments. The water window is indicated by dotted lines in which no electrolysis of water occurs. b) Collated impedance spectroscopy of the same four LCGO electrodes along with equivalent circuit modeling (inset). Error bars indicate standard deviation of the data collected at each frequency. c) Example of cyclic voltammetry using single LCGO electrode at several scan rates to determine the double layer capacitance (results shown in Figure S5 in the Supporting Information). d) Optical microscope image of end of LCGO electrode and 120 μm Pt/Ir wire as indicated.

Supporting Information). The lowest Q_{inj} value was calculating assuming that the electrolyte is in contact with the entire brush, as well as the tip (GSA_cone). Using this method yields a Q_{inj} of 14.2 mC cm^{-2}, which is comparable to conducting polymer electrodes fabricated with PEDOT.[47] A range of other common and experimental neural stimulation materials are compared with LCGO in **Table 1**.

The large Q_{inj} values measured for these electrodes are almost definitely a consequence of the inherent porosity and resultant large electrochemical surface area (e.g., surface roughness) (Figure 1d). To estimate this roughness factor, we consider the double-layer capacitance values measured for smooth, glassy carbon electrodes. Braun et al.[50] measured a double-layer capacitance of glassy carbon of 20 μF cm^{-2}. Glassy carbon is a microcrystalline construct of graphite exposing both edge planes and basal planes to the electrolyte, making it a reasonable model for LCGO electrodes.[50] Considering this value of 20 μF cm^{-2}, we can compare directly to the value we measure from EIS modeling, which is 15.8 mF cm^{-2} (16.1 μF/1.02 × 10^{-3} cm^2, GSA cone) if we consider our exposed electrode area to be that of a cone (largest possible overestimation of GSA). Using both of these values, we estimate a roughness enhancement factor of $15.8 \times 10^{-3}/20 \times 10^{-6} = 790$.

Q_{inj} derived from CV yielded high values of 62 mC cm^{-2} and 19 mC cm^{-2} for disc and cone GSA models, respectively. This

Table 1. Charge injection capacity value (Q_{inj}) for several materials used to fabricate neural interfacing electrodes. For LCGO, two different methods (EIS vs CV) and two different GSA values (disc vs. cone) are used to estimate Q_{inj}. Further information about this procedure is in the text.

Material	Q_{inj} [mC cm^{-2}]	Q_{inj} mechanism	Water window (vs Ag|AgCl)
Pt[a,b]	0.05–0.15[a], 0.26[b]	Faradaic/capacitive	−0.6 to 0.8 V
Roughened Pt[c]	0.13–0.364	Faradaic/capacitive	−0.6 to 0.8 V
Act-IrOx[a]	1–5	Faradaic	−0.6 to 0.8 V
CNTs[a]	1–1.6	Capacitive	−1.5 to 1.0 V
PEDOT[a]	15	Faradaic[a]	−0.9 V to 0.6 V
TiN[a]	1	Capacitive	−0.8 to 1.1 V
N-doped Diamond[d]	0.1–0.2	Capacitive	−1.1 to 1.1 V
GO-doped PEDOT[e]	1–4.5	Faradaic	−0.6 to 0.6 V
LCGO[b]	46 ± 2.9 (n = 4) [EIS_Disc]	Capacitive	−1 to 0.9 V
	14 ± 0.9 (n = 4) [EIS_Cone]		
	62 ± 5.1 (n = 4) [CV_Disc]		
	19 ± 1.6 (n = 4) [CV_Cone]		

References from table: [a]Cogan,[47]; [b]this work; [c]Green et al.,[48]; [d]Garrett et al.,[49]; [e]Tian et al.[37]

method is illustrated in Figure S5 (Supporting Information). These results are similar to those calculated using EIS models, though slightly larger. Direct current (DC) techniques such as CV, however, are generally not considered an accurate model for stimulation electrodes due to the short pulse times used during neural stimulation protocols. EIS uses a range of alternating current (AC) frequencies to capture, broadly, the electrochemical phenomena occurring at the electrode in the solution. Finally, for comparison and validation of our method, we performed EIS on a 200 µm diameter Pt disc electrode using the same setup (Figure S4, Supporting Information). We modeled the Pt electrode with an equivalent circuit and extracted a C_{dl} of 0.46 mF cm^{-2}. Using Equation (1), we calculated the Q_{inj} of Pt as 0.26 mC cm^{-2}—comparable to literature values (Table 1). The value is slightly inflated from those typically observed for smooth Pt surfaces because the electrode was cut with a razor blade to remove the insulation, thereby roughening the surface and potentially exposing more Pt to solution than just a disc electrode.

2.3. Retinal Ganglion Cell Stimulation

A whole-mount retina preparation was used in conjunction with intracellular patch clamp recording to determine the safety and efficacy of stimulating neuronal tissue with LCGO electrodes (**Figure 4**a). The LCGO electrode, isolated with 259 mW laser power, was lowered using a micromanipulator until the retina was visibly indented. Biphasic current pulses (500 µs/phase) were delivered through the LCGO electrode, while a whole-cell patch clamp recording was used to monitor spiking activity of a single RGC. The amplitude of the current pulse was increased until 100% efficacy was achieved (Figure 4c). A logistic fit was used to determine threshold-to-50% efficacy (b in Equation (2)). The response probability $P(R = 1|S)$ was determined by fitting the data to the logistic function

$$P(R=1|S)=\frac{d}{1+e^{-a(\mathrm{Amp}+b)}} \tag{2}$$

where d is a proportionality constant between 0 and 1, Amp is the amplitude of the biphasic pulse used to stimulate the tissue, a is a constant controlling how rapidly the spike probability increases, and b is the value of Amp for which half of the maximal value of the spike probability is achieved.

This procedure was performed for n = 8 RGCs, yielding an average b of 103 ± 87 µA using 500 µs pulse width, which means $5.1 \times 10^{-2} \pm 4.3 \times 10^{-2}$ µC were injected into the tissue, which is well within the electrolysis limits for this electrode (Table 1). The charge density required for 50% stimulation is 90 µC cm^{-2} for an electrode having a radius of 95.4 µm. A model for safe tissue stimulation was proposed by Shannon[51]

$$\log\left(\frac{Q}{A}\right)=k-\log(Q) \tag{3}$$

where Q is charge per phase, A is electrode geometrical surface area, and k is a constant derived from experiments where

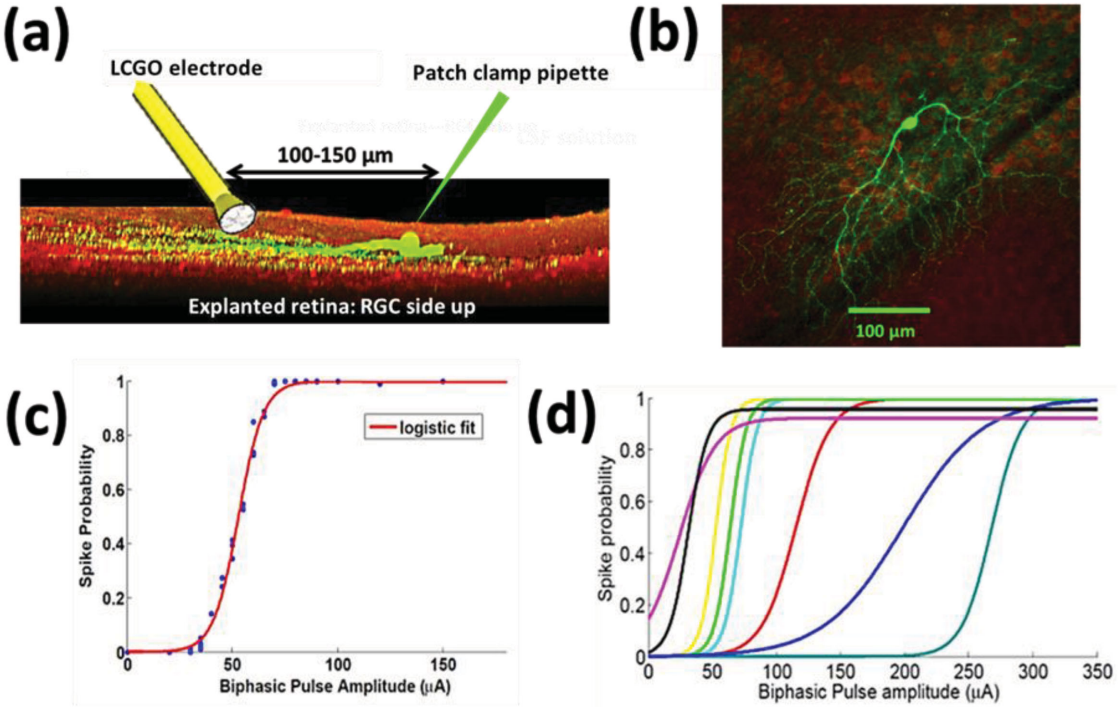

Figure 4. In vitro electrophysiology using LCGO stimulating electrodes. a) Whole retinas were explanted and placed retinal ganglion cell side up in a perfusion chamber. The LCGO electrodes were placed on the inner limiting membrane, while patch clamp recordings were acquired from individual RGCs. b) 3D reconstruction of a sample RGC. c) Response probability for a sample cell. The blue dots show the raw probability (ratio of number of direct response to total number of stimuli) and the red line shows a sigmoidal curve fit. d) Sigmoidal curve fits for all eight RGCs stimulated.

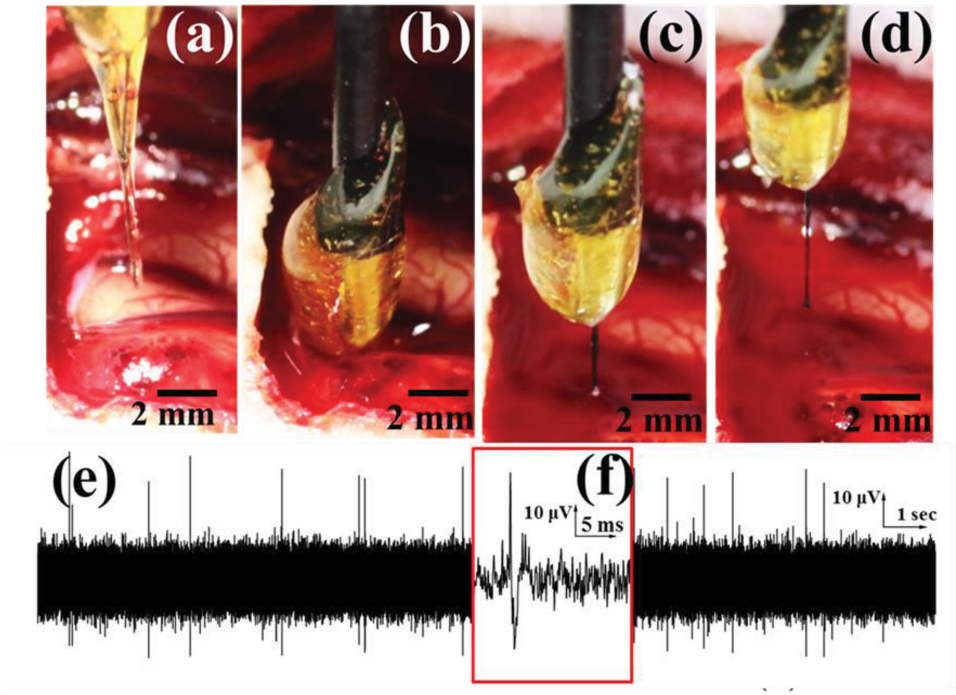

Figure 5. Flexible electrode insertion into feline visual cortex. a) LCGO electrode is coated in a rigid sucrose carrier needle and b) implanted into the brain. c,d) LCGO electrode was removed from brain after 15 min of recording; sugar needle is completely dissolved. e) Neural activity recorded within 20 s of implantation, confirming sucrose dissolution. f) Magnified image of action potential recorded with LCGO electrode.

the boundary between safe and unsafe tissue stimulation was determined. According to Equation (3), the LCGO electrode *k*-value is 0.668 for stimulation of RGCs. According to this model, the stimulation protocol used in this work to activate RGCs lies well within the safe limit for disc electrodes (k = 1.5). In reality, the charge density will be less as the electrolyte is undoubtedly able to penetrate within the brush leading to a spreading of the charge across a much larger area than a confined disc. Using Shannon's model, it can also be determined that safe stimulation is linearly related to electrode diameter rather than electrode area. This effect is likely due to the "edge effect" of disc electrodes in which larger current densities are experienced at the outer perimeter of the electrodes. The LCGO electrodes described here have a unique ''brush" conformation that may negate the edge effect, though a further investigation is required.

2.4. In Vivo Implantation of LCGO Electrode

An LCGO electrode was coated with a water-soluble sucrose microneedle. This method of forming a microneedle has been previously employed for drug delivery, as well as flexible polyimide electrode insertion into neural tissue.[21,43] Spontaneous neural bursting activity was observed approximately 30 s after electrode implantation, suggesting sugar dissolution and exposure of electrode active site. The sugar dissolved much more quickly in the brain than it did in the benchtop test with room temperature tap water because sugar's solubility in water increases with temperature. The LCGO electrode was extracted from the brain after a 15 min recording window and was still structurally intact. Additionally, the sugar had completely dissolved around the shank and electrode tip. **Figure 5** illustrates both the insertion and extraction of the sucrose-coated LCGO electrode and includes a sample of neural recording.

Though this electrode was originally intended for neural stimulation applications, the implantation experiment revealed the potential to make high quality recordings from neural populations in the brain using LCGO electrodes. This opens up the possibility of closed-loop neural interfaces in which stimulation electrodes can also be used for recording. It is obvious from Figure 5c,d that electrode insertion led to bleeding. The fabrication of sugar needles, as well as insertion procedures, should be improved markedly to avoid such trauma in future applications.

3. Conclusion

It is strongly suggested, both empirically and theoretically, that small, mechanically compliant electrodes should comprise the next generation of neural interfaces.[18] Although there are several materials that possess favorable electrochemical, surface, mechanical, and electrical properties, their fabrication and incorporation into biomedical devices remains a challenge. In this work, we use wet-spun reduced GO fibers to fabricate electrodes for electrochemical characterization and electrophysiology experiments. While a majority of conductive, compliant materials—such as conductive polymers and hydrogels—are electrodeposited onto dense, rigid substrates such as Pt or Au microwires, high strength fibers such as the ones presented here can function as free-standing penetrating electrodes. Using parylene-C as a biocompatible insulator and laser

ablation to selectively open and expand the end of the fiber, we have fabricated a freestanding, flexible, small diameter shank that is seamlessly attached to a large diameter (≈200 µm) brush-like electrode. Using this process, there is no need for welding a larger electrode onto the end of a small diameter wire, nor is there any interface between mismatched materials. Both EIS and CV confirm that the LCGO electrodes have high charge injection capacity in the range of tens of mC cm^{-2}. We demonstrate that the electrodes are effective at stimulating RGCs and can be inserted into cortex by encasing the electrodes in a water-soluble sucrose microneedle. Spiking activity was recorded from cortex confirming that the needle had dissolved and that the electrode was active. The high quality recording we observed makes these electrodes a promising candidate for electrode arrays that can stimulate or recording using any electrode, thus enabling closed-loop, self-regulating implantable devices.

4. Experimental Section

Electrode Fabrication: Wet-spinning of GO fibers was carried out with a custom-built wet-spinning apparatus and $CaCl_2$ as a coagulation bath as described previously.[40] Dried GO fibers were obtained by air drying under tension at room temperature. Reduced fibers were prepared by overnight annealing at 220 °C under vacuum. Reduced fibers (40–50 µm diameter) were cut into 8–10 mm pieces and attached to copper wires using conductive Ag epoxy (ITW Chemtronics, CW2400). Electrodes were coated with 2 µm of Parylene-C in a thermal evaporator (Labcoter 2; Specialty Coatings Systems, Inc). Removal of insulation was performed using a Nd:Yag 532 nm laser (Oxford Lasers) at a frequency of 5000 Hz, feed rate of 1 mm s^{-1}, and powers ranging from 67 to 249 mW. Laser power was chosen as a percentage of attenuated power, but was measured immediately before each cut was made due to fluctuations in diode power. For comparison, Pt/Ir (90/10) wire electrodes having 200 µm diameter were attached to copper wires and insulated with acrylic paint, but were exposed using a blade to remove end of wire rather than a laser.

Electrochemistry: Cyclic voltammetry and EIS were performed in a three-electrode electrochemical cell. The electrolyte solution was room temperature (25 °C), pH 7.4, 50×10^{-3} M phosphate buffered saline (PBS). An Ag/AgCl reference electrode (CHI Instruments, Inc), a large surface area platinum auxiliary electrode, Solatron SI1287 potentiostat, Solartron SI1260 Impedance/Gain-Phase analyzer were used for CV and EIS. Corrware/Corrview and Zplot/Zview software (Scribner Associates, Inc.) were used for instrument control and visualization of results. Distance between reference and working electrodes was kept at 2–3 cm for all measurements. Three consecutive CV sweeps from 0 to 1.6 V versus Ag/AgCl at 50 mV s^{-1} were employed to clean the electrode surface following laser ablation, while sweeps from –1.7 to 1.5 V were used to determine the water window (e.g., threshold to electrolysis) of LCGO electrodes. EIS using a 50 mV amplitude sinusoidal voltage was used to characterize charge transfer characteristics of electrodes, determine the extent of parylene-C removal on the LCGO electrodes following laser ablation, and ultimately develop an equivalent circuit model.

Stimulation of Retina: Whole cell intracellular data came from Long-Evans rats ranging from 1 to 6 months in age. Methods conformed to the policies of the National Health and Medical Research Council of Australia (NHMRC) and were approved by the Animal Experimentation Ethics Committee of the University of Melbourne (Ethics Approval #: 1112084). Animals were initially anesthetized with a mixture of ketamine and xylazine prior to enucleation. After enucleation, the rats were sacrificed with an overdose of pentobarbital sodium (intracardiac). Dissections were carried out under dim light conditions. After hemisecting the eyes behind the ora serrata, the vitreous bodies were removed, and the retinas cut into two pieces. The retinas were left in a perfusion dish with carbogenated Ames medium (Sigma) at room temperature. Pieces of retina were mounted onto a glass slide, ganglion cell layer up, and held in place with a perfusion chamber and stainless-steel harp fitted with Lycra threads (Warner Instruments). Once mounted in the chamber, the retina was perfused (4–6 mL min^{-1}) with carbogenated Ames medium at room temperature. LCGO stimulating electrodes were lowered onto the retina, until a slight depression on the retina was observed, and placed 150–200 µm away from the RGC of interest (Figure 4a). Whole cell intracellular recordings were obtained using standard procedures.[52] Intracellular recordings (n = 8) were obtained while cells were stimulated with a train of 100 biphasic pulses of fixed amplitude from the extracellular stimulating electrode. After each stimulus train, the amplitude of the biphasic pulse was increased and applied to the tissue. Responses were recorded and determined to be "stimulus evoked" if they were within 5 ms of the delivered stimulus. Following recordings, cells were fixed, stained, and imaged using confocal microscopy and 3D reconstruction.[53]

In Vivo Implantation of LCGO Electrodes: Methods conformed to the policies of the National Health and Medical Research Council of Australia and were approved by the Animal Ethics Committee of the Victorian Eye and Ear Hospital. An LCGO electrode was coated with a sucrose microneedle vehicle using a drawing lithography technique.[21,43] An anesthetized adult, male feline was placed in a stereotaxic frame and a craniotomy was performed over the visual cortex. The dura mater was removed carefully and the wound irrigated with sterile saline. The LCGO electrode was positioned with a micromanipulator and inserted into the tissue at a velocity of 4 mm s^{-1} (see supplementary 3, Supporting Information: Video of Surgical Insertion). A platinum needle electrode was placed in the skin folds at the back of the neck and used as a reference for recording. Recordings were made immediately following implantation of the electrode using a Bioamp (World Precision Instruments ISO-80). After a 15 min recording period, the electrode was retracted slowly initially in bursts, and then removed at 4 mm s^{-1}. Neural tracings were bandpass filtered (300–5000 kHz) and spikes were counted in IgorPro (Wavemetrics).[54]

Supporting Information

Supporting Information is available from the Wiley Online Library or from the author.

Acknowledgements

The Bionics Institute acknowledges the support they receive from the Victorian Government through its Operational Infrastructure Program. N.V.A. was supported by an MMI-CSIRO Material Science Ph.D. Scholarship. D.J.G. was supported by ARC DECRA Grant DE130100922. This research was supported by the Australian Research Council (ARC) through its Special Research Initiative (SRI) in Bionic Vision Science and Technology grant to Bionic Vision Australia (BVA). J.F. was supported by the Australian Research Council under Discovery Early Career Researcher award (Javad Foroughi DE1201051712). M.R.I. was supported by the Centre of Excellence for Integrative Brain Function (CE140100007). G.G.W. acknowledges ARC Laureate Fellowship and support through the ARC Centre of Excellence for Electromaterials Science.

Received: January 9, 2015
Revised: March 29, 2015
Published online: May 4, 2015

[1] a) B. Wilson, M. Dorman, *J. Rehabil. Res. Dev.* **2008**, *45*, 695; b) B. S. Wilson, C. C. Finley, D. T. Lawson, R. D. Wolford, D. K. Eddington, W. M. Rabinowitz, *Nature* **1991**, *352*, 236.

[2] D. B. McCreery, *Hearing Res.* **2008**, *242*, 64.
[3] a) K. Ganesan, D. Garrett, A. Ahnood, M. Shivdasani, W. Tong, A. Turnley, K. Fox, H. Meffin, S. Prawer, *Biomaterials* **2014**, *35*, 908; b) M. Humayun, J. Weiland, D. Nanduri, *Neurosci. Retinal Prosthesis New Visual Neurosciences*, MIT Press Camridge USA **2014**, 1627; c) J. Weiland, W. Liu, M. Humayun, *Annu. Rev. Biomed. Eng.* **2005**, *7*, 361.
[4] a) S. P. Levine, J. E. Huggins, S. L. BeMent, R. K. Kushwaha, L. A. Schuh, M. M. Rohde, E. A. Passaro, D. A. Ross, K. V. Elisevich, B. J. Smith, *IEEE Trans. Rehabil. Eng.* **2000**, *8*, 180; b) A. Schwartz, *Annu. Rev. Neurosci.* **2004**, *27*, 487; c) P. Ifft, S. Shokur, Z. Li, M. Lebedev, M. A. L. Nicolelis, *Sci. Transl. Med.* **2013**, *5*, 210.
[5] a) H. Al Jehani, L. Jacques, *Peripheral Nerve Stimulation* **2011**, *24*, 27; b) J. Hamann, S. Ruble, C. Stolen, M. Wang, R. Gupta, S. Rastogi, H. Sabbah, *Eur. J. Heart Fail.* **2013**, *15*, 1319; c) A. Kent, W. Grill, *J. Neural Eng.* **2013**, *10*, 036010; d) B. Lega, C. Halpern, J. Jaggi, G. Baltuch, *Neurobiol. Dis.* **2010**, *38*, 354.
[6] W. Grill, S. Norman, R. Bellamkonda, *Annu. Rev. Biomed. Eng.* **2009**, *11*, 1.
[7] J. Groothuis, N. Ramsey, G. van der Plasse, G. M. J. Ramakers, *Brain Stimulation* **2014**, *7*, 1.
[8] N. Thakor, *Sci. Transl. Med.* **2013**, *5*, 210.
[9] K. Deisseroth, *Nat. Methods* **2011**, *8*, 26.
[10] G. McConnell, H. Rees, A. Levey, C.-A. Gutekunst, R. Gross, R. Bellamkonda, *J. Neural Eng.* **2009**, *6*, 056003.
[11] T. D. Y. Kozai, A. Vazquez, C. Lweaver, S.-G. Kim, X. T. Cui, C. Weaver, *J. Neural Eng.* **2012**, *9*, 066001.
[12] T. Saxena, L. Karumbaiah, E. Gaupp, R. Patkar, K. Patil, M. Betancur, G. Stanley, R. Bellamkonda, *Biomaterials* **2013**, *34*, 4703.
[13] P. Stice, A. Gilletti, A. Panitch, J. Muthuswamy, *J. Neural Eng.* **2007**, *4*, 42.
[14] J. Thelin, H. Jorntell, E. Psouni, M. Garwicz, J. Schouenborg, H. Jorntell, N. Danielsen, C. Linsmeier, *PLoS One* **2011**, *6*, e16267.
[15] G. Lind, C. Linsmeier, J. Schouenborg, *Sci. Rep.* **2013**, *3*, 2942.
[16] a) R. Biran, D. Martin, P. Tresco, *J. Biomed. Mater. Res. Part A* **2007**, *82*, 169; b) A. Gilletti, J. Muthuswamy, *J. Neural Eng.* **2006**, *3*, 189.
[17] J. P. Harris, A. E. Hess, S. J. Rowan, C. Weder, C. A. Zorman, D. J. Tyler, J. R. Capadona, *J. Neural Eng.* **2011**, *8*, 046010.
[18] J. K. Nguyen, D. J. Park, J. L. Skousen, A. E. Hess-Dunning, D. J. Tyler, S. J. Rowan, C. Weder, J. R. Capadona, *J. Neural Eng.* **2014**, *11*, 056014.
[19] G. Lind, C. Linsmeier, J. Thelin, J. Schouenborg, *J. Neural Eng.* **2010**, *7*, 046005.
[20] L. Tien, F. Wu, M. Tang Schomer, E. Yoon, F. Omenetto, D. Kaplan, *Adv. Funct. Mater.* **2013**, *23*, 3185.
[21] Z. Xiang, S.-C. Yen, N. Xue, T. Sun, W. Tsang, S. Zhang, L.-D. Liao, N. Thakor, C. Lee, *J. Micromech. Microeng.* **2014**, *24*, 065015.
[22] H. Zhang, P. R. Patel, Z. Xie, S. D. Swanson, X. Wang, N. A. Kotov, *ACS Nano* **2013**, *7*, 7619.
[23] L. Spataro, J. Dilgen, S. Retterer, M. Isaacson, A. J. Spence, J. N. Turner, W. Shain, *Exp. Neurol.* **2005**, *194*, 289.
[24] K. Potter, A. Buck, W. Self, M. Callanan, S. Sunil, J. Capadona, *Biomaterials* **2013**, *34*, 7001.
[25] T. D. Y. Kozai, N. Langhals, P. Patel, X. Deng, H. Zhang, K. L. Smith, J. Lahann, N. Kotov, D. Kipke, *Nat. Mater.* **2012**, *11*, 1065.
[26] L. Zhang, Z. Cao, T. Bai, L. Carr, J.-R. Ella Menye, C. Irvin, B. Ratner, S. Jiang, *Nat. Biotechnol.* **2013**, *31*, 553.
[27] R. Green, N. Lovell, L. Poole Warren, *Biomaterials* **2009**, *30*, 3637.
[28] a) D. Borton, M. Yin, J. Aceros, A. Nurmikko, *J. Neural Eng.* **2013**, *10*, 026010; b) M. Yin, D. Borton, J. Aceros, W. Patterson, A. Nurmikko, *IEEE Trans. Biomed. Circuits Syst.* **2013**, *7*, 115.
[29] a) B. D. Ratner, A. S. Hoffman, F. J. Schoen, J. E. Lemons, *Biomaterials Science: An Introduction to Materials in Medicine*, Elsevier Science, Oxford **2012**; b) S. Ku, M. Lee, C. Park, *Adv. Healthcare Mater.* **2013**, *2*, 244.
[30] a) H. N. Lim, N. M. Huang, S. S. Lim, I. Harrison, C. H. Chia, *Int. J. Nanomed.* **2011**, *6*, 1817; b) S. Park, J. Park, S. Sim, M. Sung, K. Kim, B. Hong, S. Hong, *Adv. Mater.* **2011**, *23*, H263.
[31] M. Zhu, C. Zeng, J. Ye, *Electroanalysis* **2011**, *23*, 907.
[32] G. Guitchounts, J. Markowitz, W. Liberti, T. Gardner, *J. Neural Eng.* **2013**, *10*, 046016.
[33] a) M. David Pur, L. Bareket Keren, G. Beit Yaakov, D. Raz Prag, Y. Hanein, *Biomed. Microdevices* **2014**, *16*, 43; b) I. Yoon, K. Hamaguchi, I. Borzenets, G. Finkelstein, R. Mooney, B. Donald, M. Giugliano, *PLoS One* **2013**, *8*, e65715.
[34] D. Lewitus, J. Landers, J. Branch, K. Smith, G. Callegari, J. Kohn, A. Neimark, *Adv. Funct. Mater.* **2011**, *21*, 2624.
[35] A. Hadjinicolaou, R. Leung, D. Garrett, K. Ganesan, K. Fox, D. A. X. Nayagam, B. J. O'Brien, M. Shivdasani, H. Meffin, M. Ibbotson, S. Prawer, *Biomaterials* **2012**, *33*, 5812.
[36] X. Luo, C. Weaver, S. Tan, X. Cui, *J. Mater. Chem. B: Mater. Biol. Med.* **2013**, *1*, 1340.
[37] H.-C. Tian, J.-Q. Liu, D.-X. Wei, X.-Y. Kang, C. Zhang, J.-C. Du, B. Yang, X. Chen, H.-Y. Zhu, Y.-N. NuLi, C.-S. Yang, *Biomaterials* **2014**, *35*, 2120.
[38] R. Jensen, O. Ziv, J. Rizzo, *Invest. Ophtalmol. Visual Sci.* **2004**, *45*, 4191.
[39] K. C. Yung, H. Liem, H. S. Choy, Z. C. Chen, K. H. Cheng, Z. X. Cai, *J. Appl. Phys.* **2013**, *113*, 244903.
[40] R. Jalili, S. Aboutalebi, D. Esrafilzadeh, R. Shepherd, J. Chen, S. Aminorroaya Yamini, K. Konstantinov, A. Minett, J. Razal, G. Wallace, *Adv. Funct. Mater.* **2013**, *23*, 5345.
[41] a) T. Chang, V. Yadav, S. De Leo, A. Mohedas, B. Rajalingam, C.-L. Chen, S. Selvarasah, M. Dokmeci, A. Khademhosseini, *Langmuir* **2007**, *23*, 11718; b) F. Cortes Salazar, H. Deng, P. Peljo, C. Pereira, F. Cortés Salazar, K. Kontturi, H. Girault, *Electrochim. Acta* **2013**, *110*, 22; c) C. Hassler, R. von Metzen, P. Ruther, T. Stieglitz, *J. Biomed. Mater. Res. Part B: Appl. Biomater.* **2010**, *93*, 266.
[42] J.-M. Yoo, S. Negi, P. Tathireddy, F. Solzbacher, J.-I. Song, L. Rieth, *J. Neurosci. Methods* **2013**, *215*, 78.
[43] K. Lee, C. Lee, H. Jung, *Biomaterials* **2011**, *32*, 3134.
[44] A. L. G. Vandeneeden, M. Sluytersrehbach, G. J. Brug, M. Sluyters Rehbach, J. H. Sluyters, *J. Electroanal. Chem. Interfacial Electrochem.* **1984**, *176*, 275.
[45] H. Ji, X. Zhao, Z. Qiao, J. Jung, Y. Zhu, Y. Lu, L. Zhang, A. MacDonald, R. Ruoff, *Nat. Commun.* **2014**, *5*, 3317.
[46] S. Minnikanti, G. Diao, J. J. Pancrazio, X. Xie, L. Rieth, F. Solzbacher, N. Peixoto, *Acta Biomater.* **2014**, *10*, 960.
[47] S. Cogan, *Annu. Rev. Biomed. Eng.* **2008**, *10*, 275.
[48] R. A. Green, P. B. Matteucci, C. W. D. Dodds, J. Palmer, W. F. Dueck, N. H. Lovell, R. T. Hassarati, P. J. Byrnes Preston, G. J. Suaning, *J. Neural Eng.* **2014**, *11*, 056017.
[49] D. Garrett, K. Ganesan, A. Stacey, K. Fox, H. Meffin, S. Prawer, *J. Neural Eng.* **2012**, *9*, 016002.
[50] A. Braun, M. Bartsch, O. Merlo, B. Schnyder, B. Schaffner, M. Bärtsch, R. Kötz, O. Haas, A. Wokaun, *Carbon* **2003**, *41*, 759.
[51] R. V. Shannon, *IEEE Trans. Biomed. Eng.* **1992**, *39*, 424.
[52] O. Hamill, A. Marty, E. Neher, B. Sakmann, F. Sigworth, *Pflügers Arch.* **1981**, *391*, 85.
[53] R. C. Wong, S. L. Cloherty, M. R. Ibbotson, B. J. O'Brien, *J. Neurophysiol.* **2012**, *108*, 2008.
[54] M. Shivdasani, J. Fallon, C. Luu, R. Cicione, P. Allen, J. Morley, C. Williams, *Invest. Ophthalmol. Vis. Sci.* **2012**, *53*, 6291.